# GASEOUS GALACTIC HALOS AND QSO ABSORPTION LINE SYSTEMS

H. J. Mo<sup>1,2</sup> and J. Miralda-Escudé<sup>2</sup>
<sup>1</sup>Max-Planck-Institut für Astrophysik, 85748 Garching, Germany

and <sup>2</sup>Institute for Advanced Study, Princeton, NJ 08540

# ABSTRACT

A model of Lyman limit QSO absorption systems is investigated where they are produced in gaseous galactic halos with a two-phase structure: a hot phase at the halo virial temperature in approximate pressure equilibrium, and a cold, photoionized phase in the form of clouds confined by the pressure of the hot medium, and falling through it to the halo center, probably to accrete on a galactic disk. We show that the masses of these clouds must be over a relatively narrow range so that they are stable against gravitational collapse and evaporation. These masses, near  $10^6 M_{\odot}$ , also lead to a covering factor near unity. The hot phase is required to have a core radius such that its cooling time in the core is equal to the age of the halo, and the mass in the cold phase is determined by the rate at which the hot gas cools. We calculate the number of Lyman limit systems arising in halos of different masses in a CDM model and their impact parameters implied by these assumptions, and find them to be in reasonable agreement with observations. The evolution with redshift is correctly reproduced at  $z \leq 2$ , while at higher redshift we predict fewer absorbers than observed. We argue that this implies that high redshift Lyman limit systems arise in more extended infall regions. The observed low ionization systems such as MgII are well reproduced as arising from the photoionized phase, and are mostly in halos around massive galaxies, while CIV selected systems are predicted to be more commonly associated with lower mass galaxies and larger impact parameters. Some CIV can also arise from regions at intermediate temperature at the boundaries of the clouds. The hot phase may give rise to detectable absorption lines in OVI, while the column densities predicted for other highly ionized species are low and difficult to observe.

Subject headings: galaxies: formation - quasars: absorption lines

#### 1. Introduction

There is now much evidence that metal line absorption systems in QSO spectra arise from gas in galactic halos, as first proposed by Bahcall & Spitzer (1969). Recent imaging and spectroscopic observations can identify directly, at low redshift, the galaxies associated with the MgII absorption systems at typical impact parameters of  $30 \, h^{-1}{\rm Kpc}^{-1}$  (Yanny, York, & Williams 1990; Bergeron & Boissé 1991; Bergeron, Cristiani, & Shaver 1992; Bechtold & Ellingson 1992; Steidel 1993, 1995). However, the origin of the "halo gas" and its dynamical properties are not well understood.

During the process of galaxy formation, intergalactic gas must collapse and move inward through the extended dark matter halos that are observed around present galaxies. A halo of hot gas at the virial temperature will form as the kinetic energy of the infalling material is thermalized in shocks. In low mass halos, the cooling time of this hot halo gas is short compared to the dynamical time if it contains all the accreted baryons; therefore, the gas must cool until the density of hot gas decreases to a level such that the cooling time is similar to the age of the system. Due to the increased cooling rate as temperatures drop, a two-phase medium will naturally form in these conditions of rapid cooling. Clouds photoionized by a radiation background will be maintained at an equilibrium temperature  $\sim 10^4$  K, in pressure equilibrium with the hotter halo gas. These clouds could form from initial inhomogeneities in the accreting gas (which should be enhanced in repeated cycles of cooling and shock-heating of the gas moving through the halo), or from the ram-pressure stripped interstellar medium of satellite galaxies. Due to their higher density, clouds will fall to the center of the halo where they can form stars or globular clusters in spheroids, or accrete in gaseous disks giving rise to spiral galaxies (Fall & Rees 1985; Gunn 1982; Kang et al. 1990).

Even though our picture of how galaxies form is still highly incomplete, what is certain is that at some point in the past gas had to dissipate and move from the outer parts to the inner parts of galactic halos, and in this process it must have produced absorption line systems in any quasar line-of-sight intercepting galactic halos. It is clear that in order to understand galaxy formation we must first understand the physical state of the gas out of which galaxies form, and that absorption line systems are an excellent observational probe to any gas dissipating in halos. Thus, the recent observational evidence that the high column density absorption systems at  $z \lesssim 1$  arise in gaseous halos around galaxies should be a landmark for our understanding of galaxy formation. A successful theory of galaxy formation must not only explain the characteristics of luminous parts of galaxies, but it is

<sup>&</sup>lt;sup>1</sup>here  $h = H_0/[100 \,\mathrm{km \ s^{-1} \ Mpc^{-1}}]$  and we use  $H_0 = 50 \,\mathrm{km \ s^{-1} \ Mpc^{-1}}$  throughout the paper

equally important that it can account for the absorption line systems.

Based on these considerations, we consider in this paper a simple two-phase model for the gaseous structure of galactic halos. Any gas at intermediate temperatures between the halo virial temperature and the photoionization equilibrium temperature will have a very short cooling time, and should not be present in large quantities. We show that photoionized clouds confined by the pressure of the hot halo and falling towards the central galaxy can be the origin of most absorption line systems with column densities  $N_{\rm HI} \gtrsim 10^{15} - 10^{16} {\rm cm}^{-2}$ . Systems of lower column density can arise in the infall regions of halos around galaxies and smaller collapsing systems (Cen et al. 1994), although at low redshift some of them may also be produced by pressure confined clouds at large radius in galactic halos (Mo 1994). The model we are investigating here is related to the one proposed in Mo (1994). That paper has considered the properties of clouds, and the pressure of a hot phase, that are needed to reproduce the observed Ly $\alpha$  forest lines at low redshifts. Here we extend this model to high column-density systems. We also propose a model for the gaseous structure of galactic halos so that the density profile of cold clouds within a halo, and the number of absorption systems that are produced, can be predicted.

In § 2 we describe models for the density profiles of the hot and photoionized components of the gaseous halos. In § 3 we examine the physical characteristics of the photoionized clouds, and the ranges of sizes and masses that are allowed by the physical processes that can form or destroy them. In § 4 we compare the predictions of our model with the observations of the quasar absorption line systems. Our results are discussed in § 5.

#### 2. The Two-Phase Model for Gaseous Galactic Halos

In theories of hierarchical gravitational collapse for galaxy formation, it is usually assumed that luminous galaxies form at the center of dark matter halos as the gas collapses, is shocked, and cools (see White 1995 for a review). At any given epoch, halos can be parameterized by their circular velocity  $V_{\rm cir}$  at the virial radius  $r_v$ . Here, we shall use as the virial radius that which contains an average density equal to  $18\pi^2\rho_{\rm crit}=178\rho_{\rm crit}$ , where  $\rho_{\rm crit}$  is the critical density, and we assume  $\Omega=1$ . This is the density obtained for a spherical perturbation that virializes at half the radius of maximum expansion (e.g., Peebles 1980). The mass of the virialized halo is then  $M_{\rm halo}=24\pi^3\,\rho_{\rm crit}\,r_v^3$ ; using also  $V_{\rm cir}=(GM_{\rm halo}/r_v)^{1/2}$ , we have

$$r_v = \frac{V_{\rm cir} t}{2\pi},\tag{1}$$

$$M_{\text{halo}} = \frac{V_{\text{cir}}^3 t}{2\pi G},\tag{2}$$

where t is the age of the universe.

According to these theories, halos should continuously be merging and gravitationally accreting gas from the intergalactic medium. The accreted new gas should be shock-heated to the virial temperature. In halos of low  $V_{\rm cir}$ , the cooling time is shorter than the dynamical time, and much of the gas can cool before it has time to move to the center of the halo (e.g., White & Rees 1978). However, there must always be some hot gas left in the halo after rapid cooling, because once a certain fraction of the gas has cooled the density of the remaining gas will be sufficiently low for the cooling time to be longer than the dynamical time, and pressure equilibrium should be established in the hot halo (Fall & Rees 1985). The cooled gas should form clouds in pressure equilibrium with the hot gas and should then fall through the galactic halo. In the presence of an external ionizing background (as well as the X-ray emission from the halo and other ionizing radiation from local stars in the central galaxy), the clouds will remain photoionized at an equilibrium temperature near  $10^4$  K.

In a massive system where the cooling time of the hot gas is longer than the dynamical time of the halo, most of the gas does not cool rapidly. Only in the inner region, where the density is higher, the gas will radiate fast enough to cool. The subsequent evolution of the system is then related to the problem of cooling flows. The standard cooling flow model used to explain the observed structure of X-ray halos in elliptical galaxies and clusters of galaxies (see Fabian 1994 for a review) involves the formation of a multiphase medium, where the hot gas is separated in phases at different temperatures cooling independently of each other and forming clouds as they move to the center. The main difficulty of these models is that they need to assume that all the phases are comoving, when in fact the densest phases should rapidly fall to the center (e.g., Balbus & Soker 1989; Loewenstein 1989; Malagoli et al. 1990). Although a thermal instability may exist in the presence of magnetic fields (Loewenstein 1990; Balbus 1991), it is not clear if relative motions can be prevented when the overdensities of different phases become large, and if clouds can ever form in cooling flows. Once formed, clouds should either turn into stars as they move through the halo, or otherwise coalesce in a gaseous disk where they are supported by angular momentum. The latter process should lead to a spiral galaxy, but it clearly does not take place in the X-ray halos where cooling is observed, which are known observationally to contain very gas-poor, giant ellipticals. The only possibility is then that clouds turn into stars in the halo, but the stellar mass function must be very different from that in normal galaxies: massive stars must be suppressed in order to avoid a very luminous young population of stars, which is not observed in the giant ellipticals in the center of X-ray halos with large cooling rates.

An alternative possibility is that there is a central adiabatic core in X-ray halos where

energy is injected by a central source. Tabor & Binney (1993) have proposed this model for elliptical galaxies, where the energy may arise from an active galactic nucleus. In disk galaxies, the energy may arise from supernova explosions. Observations of "superbubbles" above the disk of our galaxy indicate that some of the energy from supernovae is indeed released into the halo (Tenorio-Tagle et al. 1990). Simple calculations show that the total energy released in supernova explosions in normal spiral galaxies is similar to the thermal energy of all the gas accreted: for a galaxy like the Milky Way, a total of 10<sup>8</sup> supernovae can produce  $\sim 10^{59}$  ergs of energy, while an accreted baryon mass of  $10^{11} M_{\odot}$  with a velocity dispersion  $\sim 200 \, \mathrm{km \ s^{-1}}$  has a thermal energy of  $10^{59}$  ergs. When a sufficient amount of hot gas is produced near the center, the halo will be globally unstable to convection, and this will set up an adiabatic core extending to a radius that should increase with the amount of energy released. As the accreted gas reaches the adiabatic core, it may cool and form photoionized clouds that fall through the adiabatic substrate, eventually being deposited in a gaseous galactic disk, or evaporating into the hot gas. This could be a way to generate a hot component with a large core radius, while a cold component moving through accretes to the galaxy disk.

In the following, we consider a simple phenomenological model for these two components of gaseous galactic halos, which should hopefully capture the essence of their structure.

### 2.1. The hot phase

Let us consider the profile of the hot gas in a halo after a time  $t_M$  since the last big merger. In other words, we assume that a large amount of gas was accreted into the system at the time of the merger, and that during the time  $t_M$  since then there has only been a much lower rate of accretion. We also assume that the feed-back effect from the central part of the halo does not alter the properties of gas at large radius. We consider first the case where the cooling time at the virial radius  $r_v$  is longer than  $t_M$ , and  $t_M$  is longer than the dynamical time. In this case, the gas at large radius should preserve its initial density after virialization, since cooling is not very important. Numerical simulations of the formation of halos show that the gas profile will approximately follow the mass profile, with a slope close to isothermal (e.g., Evrard 1990, Navarro, Frenk, & White 1995); thus, we assume that the density of hot gas is  $\rho_h \propto r^{-2}$  at large radius. There will then be a radius  $r_c$  ( $< r_v$ ) where the cooling time is equal to  $t_M$ , which we call the cooling radius.

At  $r < r_c$ , the density profile must be shallower than isothermal, because otherwise most of the cooling radiation would be emitted near the center. In cooling flow models, and when the gravitational potential is important, the core radius of the gas profile is similar to the cooling radius (Waxman & Miralda-Escudé 1995). In general, the detailed density

profile of the hot gas depends on the initial conditions of the assumed multiphase gas when it starts cooling (Nulsen 1986). A narrow initial temperature distribution will result in a steep gas density profile ( $\rho_h \propto r^{-3/2}$  for an isothermal potential well). This does not result in a good model for galactic halos, since it produces an X-ray surface brightness much higher than observed. A more extended profile for a cooling flow model can be obtained when the hot gas forms a multiphase medium with a wide temperature distribution. The flattest possible density profile occurs when the temperature profile is adiabatic. An adiabatic temperature profile can also be produced by the presence of a central energy source, as described previously. For simplicity we will adopt a model where the adiabatic halo extends all the way to the cooling radius  $r_c$ . This gives the flattest core that is consistent with the convective stability of the hot halo, if the profile outside  $r_c$  is isothermal.

In such an adiabatic halo, the pressure of the hot gas  $P_h$  is related to  $\rho_h$  by  $P_h \propto \rho_h^{5/3}$ . From the equation of hydrostatic equilibrium in an isothermal sphere it then follows that the density and temperature profiles are given by

$$\rho_h(r) = \rho_h(r_c) \left[ 1 - \frac{2}{5} \frac{\mu V_{\text{cir}}^2}{k T_h(r_c)} \ln \frac{r}{r_c} \right]^{3/2}; \tag{3}$$

$$T_h(r) = T_h(r_c) \left[ 1 - \frac{2}{5} \frac{\mu V_{\text{cir}}^2}{k T_h(r_c)} \ln \frac{r}{r_c} \right], \tag{4}$$

where  $\mu$  is the average mass per particle. We assume that the temperature of the hot gas at the cooling radius  $r_c$  is equal to the virial temperature, so that  $T_h(r_c) = T_v \equiv \mu V_{\text{cir}}^2/2k$ . The density of hot gas at  $r_c$ ,  $\rho_h(r_c)$ , is obtained by requiring the cooling time at  $r_c$  be equal to  $t_M$ :

$$\rho_h(r_c) = \frac{5\mu \, kT_v}{2\Lambda(T_v)t_M},\tag{5}$$

where  $\Lambda$  is the cooling rate. To determine  $r_c$ , we assume

$$\rho_h(r_c) = \frac{f_g V_{\text{cir}}^2}{4\pi G r_c^2},\tag{6}$$

so that the density of hot gas at this radius is a fraction of  $f_g$  of the total density of the halo.

When  $r_c > r_v$ , the cooling time at the virial radius is already short compared to  $t_M$ , and the fraction of gas in the hot phase is small. In this case, the cooling radius  $r_c$  defined by equations (5) and (6) is simply a parameter rather than a physical cooling radius. We assume that the residual hot gas at  $r_v$  is still at the virial temperature and has a density such that its cooling time is equal to  $t_M$ , so that  $T_h(r_v) = T_v$  and  $\rho_h(r_v) = (5\mu kT_v)/[2\Lambda(T_v)t_M]$ . For simplicity we also assume that the hot gas within  $r_v$  has density and temperature

profiles similar to those described by equations (3) and (4), but with  $r_c$  replaced by  $r_v$ . Outside  $r_v$ , the gas has typically not been shocked and not much hot gas should exist there.

The time  $t_M$  in equation (5) corresponds to the interval between major mergers, since the gas is then heated to a stage from which it starts cooling. This time depends on the halo mass and the power spectrum; we ignore this complication here, and assume  $t_M = t/(1+\Omega)$ , where t is the age of the universe. This reproduces an earlier formation of halos for low  $\Omega$  (see also Fig.8 of Lacey & Cole 1993 for  $\Omega = 1$ ). The result obtained for the cooling radius in terms of the halo circular velocity is shown in Figure 1 at several redshifts, assuming  $f_g = 0.05$  and a metallicity  $Z = 0.3Z_{\odot}$  for the cooling function adopted from Sutherland & Dopita (1993). For typical  $L_*$  galaxies ( $V_{\rm cir} \simeq 250\,{\rm km~s^{-1}}$ ) at  $z \sim 0$ , the cooling radius is near 150 Kpc, and it stays almost constant as we increase the halo velocity, up to scales of rich clusters of galaxies. For smaller galaxies, the cooling radius is larger and eventually reaches the virial radius; the value of  $V_{\rm cir}$  at which this occurs is shown by the thick vertical ticks in Figure 1.

The total surface brightness emitted in soft X-rays by these hot halos can be computed given the emissivity per unit volume,  $\epsilon_x(r) = \epsilon_0 \rho_h^2(r)/\mu_e^2$ , where  $\mu_e$  is the gas mass per electron. The result is:

$$S_x(R) = \frac{2\epsilon_0 f_g^2 V_{\text{cir}}^4}{64\pi^3 G^2 \mu_e^2 r_c^3} F(R/r_c)$$

$$= 1.5 \times 10^{-8} \left(\frac{f_g}{0.05}\right)^2 \left(\frac{V_{\text{cir}}}{200 \,\text{km s}^{-1}}\right)^4 \left(\frac{100 \,\text{Kpc}}{r_c}\right)^3 F\left(\frac{R}{r_c}\right) \,\text{erg cm}^{-2} \,\text{sec}^{-1} \,\text{sr}^{-1}, \qquad (7)$$

where R is the radius in projection and, for the density profile given by equation (3), the dimensionless function F is  $F(x) = \int_0^1 dz \left[1 - (2/5) \ln (z^2 + x^2)\right]^2$ , where we have neglected the minor contribution from the gas outside the adiabatic core. Taking the characteristic values in equation (7), and  $\epsilon_0 = 2 \times 10^{-23} \, \mathrm{erg cm^3 \, sec^{-1}}$ , (adequate for temperatures  $\sim$  few  $10^6 \, \mathrm{K}$  and  $Z \sim 0.1 Z_{\odot}$ ), we find that for halos with  $r_c = 100 \, \mathrm{Kpc}$  the surface brightness at  $R = 100(20) \, \mathrm{Kpc}$  is  $S_x = 1.5 \times 10^{-8} (4 \times 10^{-8}) \, \mathrm{erg cm^{-2} \, sec^{-1}}$  sr<sup>-1</sup>, and the total luminosity within  $r_c$  is  $L_x \sim 7 \times 10^{40} \, \mathrm{erg \, sec^{-1}}$ .

The value for the surface brightness obtained at radii  $R \sim 20 \,\mathrm{Kpc}$  is consistent with the observational upper limits. For example, McCammon & Sanders (1984) find that the X-ray surface brightness within 30 Kpc around the galaxy M101 (where the disk circular velocity is  $V_{\rm cir} \simeq 200 \,\mathrm{km \ s^{-1}}$ ; Dean & Davies 1975) is smaller than  $\sim 3 \times 10^{-8} \,\mathrm{erg cm^{-2} \, sec^{-1}}$  sr<sup>-1</sup>, corresponding to  $L_x < 10^{40} \,\mathrm{erg \, sec^{-1}}$  within the same radius. This upper limit was determined by subtracting the emission between 30 and 50 Kpc from the emission within 30 Kpc, so for a very extended X-ray halo the central surface brightness could probably be larger. For our galaxy, the emission measure that is derived from the hot gas at radius  $\sim 100 \,\mathrm{Kpc}$  is  $\sim 2 \times 10^{-3} \,\mathrm{pc \, cm^{-6}}$ , which is consistent with the soft X-ray background (e.g.

Wang & McCray 1993). Despite of this, it is clear that the density profile of the hot gas cannot be much steeper than that assumed in our model. The hot phase in our model (and the large total X-ray luminosity it produces) is still consistent with the X-ray observations of normal galaxies only because we have assumed a large core radius for the hot gas.

It is possible that  $f_g$  is substantially smaller than 0.05, and a steeper density profile is then allowed. However, the value of  $f_g$  in our model is also constrained by the absorption line systems, as will be discussed later in the paper.

# 2.2. The cold phase

The accreted gas that does not stay in the hot phase and cools must fall through the hot halo in the form of photoionized clouds. We refer to the gas in these clouds as the "cold phase". As discussed before, the rate at which cold gas accumulates in a halo is determined by both gas infall and gas cooling. The accumulation rate is in general not uniform in time: it may be substantially higher than the average during a big merger when large amount of gas is accreted and can cool. We shall, however, ignore this in our simple model.

In small halos, where the cooling time of the hot gas within the virial radius is much shorter than the dynamical time, most of the accreted gas will have cooled. Since the total gas mass accreted in a halo with circular velocity  $V_{\rm cir}$  is  $f_g V_{\rm cir}^2 r_v / G$ , the total mass of gas that has been in the cold phase can be written as

$$M = \frac{f_g V_{\text{cir}}^2 r_v}{G} - \int_0^{r_v} 4\pi x^2 \rho_h(x) \, dx, \tag{8}$$

where  $\rho_h(x)$  is the density of gas in the hot phase, as discussed in §2.1. For massive halos where the cooling time in their outer region is longer than the dynamical time, we assume that the infalling gas is initially shock-heated to the virial temperature, and cold gas results from subsequent cooling. In this case, the total mass of gas that has been in the cold phase can approximately be written as

$$M = \frac{f_g V_{\text{cir}}^2 r_c}{G} - \int_0^{r_c} 4\pi x^2 \rho_h(x) \, dx, \tag{9}$$

where we have assumed that the amount of cold gas outside  $r_c$  is negligible.

We now assume that most of the cold gas has been formed near a radius  $r_{min} \equiv \min(r_v, r_c)$ , and that a constant mass inflow rate of the cold gas is present within  $r_{min}$ , and no cold gas is present outside this radius. This approximation is adequate when there is heated gas in an adiabatic core, since the accreting gas would then start forming clouds at  $r_c$  when it mixes with the heated gas, and in a cooling flow model where, for a

wide initial temperature distribution, most of the gas is deposited near  $r_c$ . The cold gas should form clouds that will fall through the halo, and it will therefore stay in the cold phase only for a short time, before forming stars or merging with the disk being formed in the halo center. We assume the mass flow rate to be  $\dot{M} = M/t_M$ , and that the clouds move to the halo center with a constant velocity  $v_c$ . Assuming also spherical symmetry for the gas distribution, we can write the density of the cold gas as a function of the distance r to the halo center as

$$\rho_c(r) = \frac{\dot{M}}{4\pi r^2 v_c} = \frac{f_g V_{\text{cir}}^2 r_{\text{min}}}{4\pi G t_M r^2 v_c} \left[ 1 - \frac{r_{\text{min}}^2}{r_c^2} \int_0^1 x^2 \left( 1 - \frac{4}{5} \ln x \right)^{3/2} \right] . \tag{10}$$

In the absence of a hot phase, the cold gas is in free fall and  $v_c$  must be of the order of the virial velocity  $V_{\rm cir}$ . The friction of hot gas may cause cold clouds to move at a terminal velocity which is smaller than  $V_{\rm cir}$ . However, since halos on galactic scales have cooling times that are similar to the dynamical times, the inflow velocity should not be much smaller than the virial velocity (see §3). The inflow velocity could be much smaller than  $V_{\rm cir}$  in massive systems, and also if relative motions of different phases could be prevented by a magnetic field. For simplicity, we will assume  $v_c$  to be a constant throughout a halo and to have a value of the order of  $V_{\rm cir}$ . We will examine the effect of changing the value of  $v_c$ .

# 3. Properties of the Clouds

The cold (photoionized) gas component of galactic halos, for which we have described a model of the average density profile in §2.2, should be in the form of clouds. We consider various physical processes affecting the formation and destruction of the clouds, and examine the range of cloud masses that are allowed.

We model the clouds as spheres of uniform, isothermal photoionized gas confined by the pressure of the hot medium, with mass  $M_c = M_5 \times 10^5 M_{\odot}$ , temperature  $T_c = T_4 \times 10^4 K$ , and pressure  $P/k = P_2 \times 10^2 \,\mathrm{K\,cm^{-3}}$ . We define the quantity:

$$Q \equiv \frac{M_c}{M_{\text{crit}}} = M_c G^{3/2} \left(\frac{P}{1.4}\right)^{1/2} \left(\frac{kT_c}{\mu}\right)^{-2} = \frac{M_5}{5.6 \times 10^3} \frac{P_2^{1/2}}{T_4^2} , \qquad (11)$$

where  $M_{\rm crit}$  is the critical mass for gravitational collapse of a cloud that is isothermal and spherical (Spitzer 1978), and  $\mu$  is the average mass per particle. For  $Q \ll 1$ , the cloud pressure is uniform, and for Q > 1 the cloud is unstable to gravitational collapse. Since the cloud is in pressure equilibrium with a hot medium of density  $\rho_h(r)$  and temperature  $T_h$ , the cloud radius is  $R_c = (3M_c/4\pi\rho_h)^{1/3}(T_c/T_h)^{1/3}$ . It is useful to define the radius

$$R_h \equiv \left(\frac{kT_h f_g}{G\rho_h \mu}\right)^{1/2} . \tag{12}$$

The quantity  $(kT_h/\mu)^{1/2}$  is the gas velocity dispersion, while  $(f_g/G\rho_h)^{1/2}$  should be of the order of the free-fall time if the hot gas has a fraction  $f_g$  of the total mass. Thus, outside the core of the hot phase, where the gas mass fraction is close to  $f_g$ ,  $R_h$  is similar to the radius r where the cloud is, and as the radius is decreases below  $r_c$ ,  $R_h$  should become larger than r since it decreases only as  $[T_h(r)\rho_h(r)]^{-1/2}$  with radius. The radius of the cloud can then be written as:

$$R_c = 0.66 Q^{1/3} f_g^{-1/2} (T_c/T_h) R_h . {13}$$

Given the profile of the average density of cold gas in a halo,  $\rho_c(r)$  (see § 2.1), the covering factor C of the clouds at a given impact parameter r is:

$$C = \pi R_c^2 l \frac{\rho_c(r)}{M_c} = 1.1 \, Q^{-1/3} \, f_g^{1/2} \frac{\rho_c(r)}{\rho_h(r)} \frac{l}{R_h} \,, \tag{14}$$

where l is the typical size of the absorbing region. The covering factor decreases with Q. Since  $R_h \gtrsim l$ , we see that if the average density in cold clouds is not much larger than the density of hot gas, Q needs to be smaller than one for the covering factor to be unity.

The solid line in Figure 2a shows the value of Q for which the covering factor is one, according to equation (14). We take  $f_g = 0.05$ ,  $T_4 = 1.5$ ,  $v_c = V_{\rm cir}$  (where  $v_c$ , defined in §2.2, is the velocity at which clouds move towards halo centers) and radius  $r = 30 \, h^{-1} {\rm Kpc}$ . The result is shown for halos at z = 0.5, with the metallicity of the hot gas  $Z = 0.3 Z_{\odot}$ . For halos with small  $V_{\rm cir}$ , higher values of Q are sufficient for a covering factor of unity, due to a larger ratio of  $\rho_c/\rho_h$  (see eq. 14). The dot-dashed line corresponds to a constant cloud mass of  $10^5 M_{\odot}$ . Figure 2b shows the same quantities but at a radius  $r = 60 \, h^{-1} {\rm Kpc}$ . At larger radius,  $\rho_c/\rho_h$  is smaller and the covering factors are lower for a given Q.

The observations of metal-line absorption systems indicate that most lines of sight within  $\sim 30\,h^{-1}{\rm Kpc}$  from normal galaxies at  $z\simeq 0.5$  show MgII absorption (Steidel 1993), while outside this radius absorption occurs less often (i.e., the MgII equivalent width is often below the observational threshold). At the same time, the absorption line profiles typically show a few subcomponents (Petitjean & Bergeron 1990), so the covering factor of the clouds within  $r\sim 30\,h^{-1}{\rm Kpc}$  must be about a few. This says that any clouds giving rise to the absorption systems must have values of Q slightly below the solid line in Fig. 2a.

Assuming ram pressure to be the main cause of drag force on a cloud, the terminal velocity  $V_t$  of a cloud at r is approximately given by  $(V_t/V_{\rm cir})^2 \sim [\rho_c(r)/\rho_h(r)]/C$ . Using equations (3) and (10), and assuming  $v_c \sim V_t$ , we have  $(V_t/V_{\rm cir})^3 \sim (r_c^2 r_{\rm min}/r^2 r_v)/(\pi C)$ . Thus in massive halos where  $r_v \gg r_c$ ,  $V_t$  can be significantly smaller than  $V_{\rm cir}$  for clouds with C=1. For example, at  $z=0.5~V_t$  is smaller than  $V_{\rm cir}$  for such clouds at  $r=30~h^{-1}{\rm Kpc}$  only in halos with  $V_{\rm cir} \gtrsim 250~{\rm km~s^{-1}}$ . This means that clouds in galactic-sized halos should move at a velocity not much smaller than the velocity dispersions of these halos.

Observations show that QSO MgII systems usually resolve into subcomponents with velocity spread typically of 100-200 km s<sup>-1</sup> (see e.g. Petitjean & Bergeron 1990). Such velocity substructures are consistent with their being produced by the motions of clouds in galactic halos.

The cloud sizes are limited by various physical processes. Clouds with Q > 1 should collapse gravitationally. In addition, sufficiently massive clouds will be self-shielding, and as the gas becomes neutral it can cool to the cold phase at  $T \simeq 50 \,\mathrm{K}$  (e.g., Ferrara & Field 1994), and can much more easily collapse gravitationally.

Small values of Q are limited by other processes. First, if the covering factor is much larger than unity the clouds will collide and coalesce as they fall through the halo. Small clouds can also be evaporated by heat conduction. In the absence of magnetic fields, this is determined by the evaporation parameter (McKee & Cowie 1977), which is essentially the ratio of the electron mean-free path to the cloud radius, and is given by

$$\sigma_{ev} = 1.2 \times 10^4 T_h^2 \,\mu/(\rho_h R_c) = 2.3 \times 10^{-3} \, \frac{V_{200}^4 \, R_{h,100}}{Q^{1/3} \, T_4 \, f_g^{1/2}} \,, \tag{15}$$

where  $V_{200} \equiv V_{\rm cir}/(200 \,{\rm km \ s^{-1}})$ , and  $R_{h,100} \equiv R_h/(100 \,{\rm Kpc})$ . Clouds with  $\sigma_{ev} \gtrsim 0.03$  will evaporate. If the evaporation is not saturated ( $\sigma_{ev} \lesssim 1$ ), as is true in our model, the evaporation time is (Cowie & McKee 1977)

$$t_{ev} = 2.2 \times 10^{10} V_{200}^{-5} Q^{2/3} T_4 \text{ yr}$$
 (16)

We have plotted as the long-dashed lines in Figure 2 the value of Q where either the cloud is radiatively stabilized ( $\sigma_0 < 0.03$ ), or the evaporation time is longer than  $r/v_c$ , so that the cloud will not evaporate as it moves through the halo over a radius r. Figure 2 shows that clouds above this evaporation line can still be small enough to have a covering factor larger than unity at an impact parameter of  $30 \, h^{-1} {\rm Kpc}$ , for halos with  $V_{\rm cir} \lesssim 230 \, {\rm km \ s^{-1}}$ . Such clouds have masses typically of about  $10^5 - 10^6 M_{\odot}$ . However, the maximum covering factor of clouds surviving evaporation is lower than unity at an impact parameter twice as large, as seen in Figure 2b. The value of Q for a constant C decreases with  $V_{\rm cir}$  at  $V_{\rm cir} \gtrsim 230 \, {\rm km \ s^{-1}}$ , since for these halos the density of cold gas is determined by the cooling rate of hot gas (equation 10), which decreases with  $V_{\rm cir}$  (see Fig.1). Of course, small clouds might be magnetized and thermally insulated from the hot phase. In this case, clouds of smaller mass and with a larger covering factor could survive evaporation. This may be needed to prevent cold clouds from evaporation in massive halos with  $r_v > r_c$ , in order to have a unity covering factor at an impact parameter of about  $30 \, h^{-1} {\rm Kpc}$  (Fig.2a).

Small clouds can also be disrupted by hydrodynamic instability when they are accelerated to the terminal velocity. Pressure confined clouds moving at the sound speed

of the hot phase are disrupted on a timescale of the order of the cloud dynamic time,  $R_c (\mu/kT_c)^{1/2}$  (e.g., Murray et al. 1993). The short dashed curves in Fig.2 show the limit of Q, above which clouds will not be disrupted by hydrodynamic instability as they move through the halo over a radius r. It is clear from the figure that a cloud that is stable against heat conduction may still be disrupted by hydrodynamic instability. However, a cloud that is disrupted into smaller lumps should then be evaporated into the hot gas, which would only increase the cooling rate and thereby promote cloud formation in the hot phase. Thus, if hydrodynamic instabilities disrupt clouds, a steady state should be reached where, once the covering factor is large enough, cloud coalescence and growth from the cooling of hot gas can balance cloud disruption and evaporation. This type of equilibrium is found in numerical simulations of sheet fragmentation (e.g., Anninos & Norman 1995; see also Begelmann & McKee 1990). As shown in Fig.2a, the covering factor of such clouds is not very different from unity within a radius of about  $30 h^{-1}$ Kpc.

## 4. Implications for QSO Absorption Line Systems

# 4.1. Relation between HI and MgII systems

In this Section we calculate the average column density of HI and other metal ions at different impact parameters from a halo. To do this we need, in addition to the parameters that describe the density profiles of gaseous halos (§2) and the properties of clouds (§3), the flux of the UV background  $J(\nu)$  and the metallicity of the absorbing gas Z. We write  $J(\nu)$  in the form

$$J(\nu) = J_{-21}(z) \times 10^{-21} \left(\frac{\nu}{\nu_{\rm HI}}\right)^{-\alpha} \Theta(\nu) \text{ erg cm}^{-2} \text{ sr}^{-1} \text{ Hz}^{-1} \text{ sec}^{-1} , \qquad (17)$$

where  $\nu_{\rm HI}$  is the hydrogen Lyman limit frequency,  $J_{-21}(z)$  gives the redshift dependence of  $J(\nu)$ , and  $\Theta(\nu)$  describes departures of the spectrum from a power-law. The shape of  $J(\nu)$  depends on the spectrum of the sources of the ionizing photons, and on the absorption by intervening material in the absorption systems themselves. Here, we shall take a representative example of models where quasars dominate the background (their spectrum is assumed to approximately follow a power-law joining the observed UV and X-ray fluxes). A typical resulting spectra (see Miralda-Escudé & Ostriker 1990; Madau 1992) can be represented approximately by taking  $\alpha=0.5,\ J_{-21}(z)=0.5$  for z>2 and  $J_{-21}(z)=0.5\times[(1+z)/3]^2$  for z<2, and including a break in the spectrum at  $\nu_4\equiv 4$  Ryd (due to continuum absorption by HeII ), with  $\Theta(\nu<\nu_4)=1$  and  $\Theta_4\equiv\Theta(\nu\geq\nu_4)=0.1$ . Notice that the amplitude of this break is expected to increase with redshift; recent observational evidence from the strength of the He II forest suggests that the break is much

larger at z = 3 (Jakobsen et al. 1994). We neglect also other spectral modifications due to emission from Ly $\alpha$  clouds, as described in Haardt & Madau (1995).

Our models can predict the number of absorption systems as a function of the HI column density that should be seen in halos of different  $V_{\rm cir}$ , given the density profiles for the cold clouds of § 2, and given the ionizing radiation background. A comparison with observations is therefore only possible for systems selected from the HI column density. For the range of column densities we are interested in, these can be detected as Lyman limit systems. Although the number and evolution of Lyman limit systems has been well studied (Sargent, Steidel, & Boksenberg 1989; Storrie-Lombardi et al. 1994; Stengler-Larrea et al. 1995), it has not yet been possible to study their relationship to galactic halos owing to the small number of known systems at low redshift. However, this situation will improve as more low-redshift quasar spectra are observed with HST (see Bahcall et al. 1995).

In the meantime, the relation of absorption systems with galactic halos has only been done from MgII selected surveys, where all systems with a MgII equivalent width above a certain threshold (usually  $0.3\mathring{A}$ ) are included. The relation between a MgII equivalent width and an HI column density is complicated and should probably show a large scatter from system to system. First of all, the column density of MgII corresponding to a given equivalent width depends on the degree of saturation of the lines, and the number of subcomponents. For an unsaturated MgII line, we have  $W_{\rm MgII} \approx 0.3\mathring{A} \, (N_{\rm MgII} \, / 10^{13} {\rm cm}^{-2})$ . The components of the observed MgII lines are generally saturated (e.g., Steidel & Sargent 1992), but for  $W < 0.3\mathring{A}$  the lines are more optically thin (see Fig.8 in Petitjean & Bergeron 1990). We could then assume a corresponding limit of  $N_{\rm MgII} > 10^{13} {\rm cm}^{-2}$  for the MgII selected surveys, although systems with higher column densities but narrow components would not be included. In addition, the ratio  $N_{\rm MgII}/N_{\rm HI}$  is proportional to the metallicity, and depends also on the ionization parameter and self-shielding in the clouds.

The observations of the metallicity show a large scatter from system to system. At high redshift, the values obtained for Lyman limit systems (LLS) from photoionization models are lower than  $\sim 0.1 Z_{\odot}$  (Steidel 1990; Petitjean, Bergeron, & Puget 1992; Vogel & Reimers 1994), and at lower redshift ( $z \lesssim 1$ ), the metallicity of MgII systems can be as high as half the solar value (Bergeron et al. 1995). We will take  $Z = 0.3 Z_{\odot}$  and examine the effect of changing Z.

In Figure 3 we show  $N_{\rm MgII}/N_{\rm HI}$  as a function of the ionization parameter,  $\Gamma$  (defined as the ratio of ionizing photon number density to the total hydrogen number density), for two values of the HI column density through a cloud, and different models of the photoionizing spectrum, as shown in the figure (see eq. [17]). We have used the code CLOUDY (Ferland 1993) to calculate the relative column densities, which assumes a plane-parallel geometry. The result is shown for a fixed temperature  $T=15000\,{\rm K}$ , and for  $Z=0.3Z_{\odot}$  (the plotted

ratio scales proportionally to the metallicity). A ratio  $N_{\rm MgII}/N_{\rm HI} \simeq 10^{-4}$  corresponds to having the same threshold for detecting a halo in absorption as a Lyman limit system (which requires  $N_{\rm HI} \gtrsim 10^{17} {\rm cm}^{-2}$ ) and as a MgII system with  $N_{\rm MgII} \gtrsim 10^{13} {\rm cm}^{-2}$ . We see that  $N_{\rm MgII}/N_{\rm HI}$  depends strongly on the ionization parameter and the spectrum of the background. For  $\Gamma < 10^{-3}$ , the ratio increases with ionization parameter, since MgII can be destroyed by the charge-transfer reaction with a proton to give MgIII and HI. At higher ionization parameters, the MgII column density drops very fast owing to the ionization of MgIII to MgIV. Since the ionization potential of MgIII is 80.1eV, this occurs in the presence of photons above the HeII ionization edge. Thus, the decline of MgII with ionization parameter is reduced as the cloud becomes optically thick, or as the break at the HeII edge is increased in the spectrum of the background. Figure 4 shows the ionization parameter ( $\Gamma$ ) as a function of the halo circular velocity, according to our model for the pressure profile of § 2, for clouds at various radii in halos of different  $V_{\rm cir}$  at z=0.5. The variation of  $\Gamma$  with  $V_{\rm cir}$  is very fast (much larger than the variation with impact parameter), due to the lower pressure in low  $V_{\rm cir}$  halos.

We therefore conclude that there is a substantial uncertainty in transforming the predictions of our model for the Lyman limit systems into the predictions for the MgII selected samples of absorption systems.

#### 4.2. Lyman limit systems

Figure 5 shows the HI column density  $(N_{\rm HI})$  as a function of the impact parameter (D) for halos of various  $V_{\text{cir}}$  at z=0.5. The value of z chosen here is similar to the mean redshift of the MgII systems for which associated galaxies are identified (Steidel 1995). We take  $f_g = 0.05$ ,  $Z = 0.3Z_{\odot}$  and  $v_c = V_{\rm cir}$ . The value of  $f_g$  is chosen to match the cosmic density of baryons,  $\Omega_b = 0.0125h^{-2}$ , obtained from primordial nucleosynthesis (see Walker et al. 1991); it could be lower if much of the baryonic material accreting in galactic halos had already formed stars or was in dense gas clumps, instead of a diffuse halo. We have used the code CLOUDY to compute the ionization fraction of hydrogen atoms, assuming a plane-parallel slab with  $N_{\rm HI} = 10^{17} {\rm cm}^{-2}$ . Because of self shielding, the column density may be significantly underestimated for  $N_{\rm HI} \gtrsim 10^{17.5} {\rm cm}^{-2}$ ; the overestimate of  $N_{\rm HI}$  at  $N_{\rm HI} < 10^{17} {\rm cm}^{-2}$  is not significant. The horizontal line shows  $N_{\rm HI} = 10^{17} {\rm cm}^{-2}$ , above which a Lyman limit system (hereafter LLS) is produced. The HI column density obviously decreases with impact parameter, because  $N_{\rm HI}$  is proportional to the total column density of cold gas, which is higher for a smaller impact parameter, and to the pressure (since neutral fraction increases with pressure), which is higher near the center. The figure shows that the impact parameter for producing a LLS is about  $40 \,h^{-1}{\rm Kpc}$  at  $V_{\rm cir} \sim 200 \,{\rm km~s^{-1}}$ . In halos with  $V_{\rm cir} \gtrsim 250 \, {\rm km \ s^{-1}}$ , this impact parameter is not much larger because the cooling radius is reached, and we assume that no clouds are formed outside the cooling radius.

In Figure 6 we show the impact parameter D where  $N_{\rm HI}=10^{17}{\rm cm}^{-2}$  as a function of  $V_{\rm cir}$ , for halos at z=0.5 and various choices of model parameters. For the same reasons mentioned above, the impact parameter increases rapidly at low  $V_{\rm cir}$  and then reaches an approximately constant value, near the cooling radius. The impact parameter decreases with the metallicity Z in halos where  $r_v < r_c$  (i.e., when the global cooling time is short), but increases with Z when  $r_v > r_c$ . In the first case, a lower cooling rate gives a larger pressure in the hot halo and a larger neutral fraction of hydrogen in the cold clouds. Since in this case the accretion rate of cold gas is determined mainly by gas infall rather than gas cooling (equation 8), the total amount of cold gas that can be accreted in the halo does not depend on Z. The situation is different when  $r_v > r_c$ . In this case, the accretion rate of cold gas is determined by gas cooling, and D increases with Z, because a larger Z means more gas that can cool (equation 9). The dependence of D on  $f_g$  is strong, due to the higher pressure when  $f_g$  is larger: D is reduced by a factor of about 2 when  $f_g$  decreases by the same factor.

The above result of impact parameter as a function of  $V_{\rm cir}$  is qualitatively the same as what is observed in MgII systems (Steidel 1993, 1995; Bechtold & Ellingson 1992). The observation shows that the maximum impact parameters of their MgII systems to the host galaxies increase slowly with the K-band luminosities of the host galaxies ( $L_K$ ) at  $L_K \gtrsim 0.1 L_K^*$ , and decrease rapidly with  $L_K$  at smaller  $L_K$ . Unfortunately, similar observations for Lyman limit systems have not yet been done.

When the comoving number density of halos is known, we can also calculate the statistical properties of the absorption systems (e.g., Mo, Miralda-Escudé, & Rees 1993). Here we use the Press-Schechter model (Press & Schechter 1974) to estimate the number density of halos. As an illustration, we consider the standard cold dark matter (CDM) model with  $\Omega_0 = 1$  and h = 0.5. We use the fit in equation (G3) of Bardeen et al. (1986) for the power spectrum, and normalize it so that  $\sigma_8 = 0.67$ , where  $\sigma_8$  is the linear RMS mass fluctuation in a top-hat window with a radius of  $8 h^{-1}$ Mpc.

Let us first examine the contribution to the total absorption cross section from halos with different  $V_{\text{cir}}$ . To do this we consider the cumulative number of absorption systems (with  $N_{\text{HI}} \geq N_0$ ) per unit redshift at z, produced in halos with  $V_{\text{cir}} \leq V_0$ :

$$\frac{\mathrm{d}N}{\mathrm{d}z}(z, N_0, V_0) = \frac{c}{H_0} (1+z)^{1/2} \int_0^{V_0} \pi R^2(V_{\mathrm{cir}}, z, N_0) n(V_{\mathrm{cir}}, z) \mathrm{d}V_{\mathrm{cir}}, \tag{18}$$

where  $n(V_{\rm cir}, z) dV_{\rm cir}$  is the differential comoving number density of halos at redshift z and with circular velocity  $V_{\rm cir}$ ;  $\pi R^2(V_{\rm cir}, z, N_0)$  is the cross section of a halo at redshift z, and

with circular velocity  $V_{\rm cir}$ , to produce an absorption system with  $N_{\rm HI} \geq N_0$ . Figure 7 shows  ${\rm d}N/{\rm d}z$  as a function of  $V_0$ , for z=0.5 and  $N_0=10^{17}{\rm cm}^{-2}$ . In the calculation, we have assumed that the covering factor of absorbers within the maximum impact parameters shown in Fig.6 is equal to or larger than unity. Thus, the contribution from massive halos, where the covering factor should be below unity (see Fig. 2), may be overestimated. From the figure we see that most of the absorption cross section is produced in halos with  $V_{\rm cir}=200\text{-}300\,{\rm km~s^{-1}}$ . The median value of  $V_{\rm cir}$ , below which half of the systems are produced, is about 250 km s<sup>-1</sup>. Small halos with  $V_{\rm cir}\lesssim 150\,{\rm km~s^{-1}}$  contribute only a small fraction of the total cross section. Thus, our model predicts that most LLSs at low redshifts are associated with halos of large galaxies.

In fact, the reason why we do not have a much larger contribution from even larger halos, corresponding to relatively poor clusters of galaxies, is because we assume that no clouds are produced outside the cooling radius. We have checked that if a small fraction of the hot gas (of the order of the ratio of the Hubble time to the cooling time) is in cold clouds at large radius as well, then more massive halos (with  $V_{\rm cir} \sim 500 \, {\rm km \ s^{-1}}$ ) dominate the cross section at low redshifts, and cause the number of LLS to increase very rapidly with time at present (due to the increasing number of massive halos). This would be clearly inconsistent with observations. Therefore, the data on the absorption systems imply that if any photoionized clouds existed in the outer regions of massive halos, where the cooling time is long, they should have a small covering factor.

The total number of HI absorption systems per unit redshift, dN/dz, contributed by all halos with any circular velocity is shown in Figure 8 as a function of z for systems with  $N_{\rm HI} \geq 10^{17} {\rm cm}^{-2}$ . The data points are observational results for LLSs, adopted from Stengler-Larrea et al (1995). Here again we have assumed a unity covering factor within the maximum impact parameter. For  $z \lesssim 2$  our model prediction is consistent with observation, provided  $f_g$  is not much smaller than 0.05. This shows that most of the LLSs at  $z \lesssim 2$  can be produced by clouds in galactic halos.

However, at  $z \gtrsim 3$  our model predicts only about one third of the LLSs observed. The reason for this discrepancy is that the virial radius of a halo large enough to produce Lyman limit systems at these high redshifts is small [c.f. equation 1; note also that at z=3, all halos with  $V_{\rm cir} \lesssim 300 \, {\rm km \ s^{-1}}$  have  $r_v < r_c$  (see Fig.1)], and their total cross section is simply not big enough. To see this more clearly, we note that at z=3 the comoving number density of halos with  $V_{\rm cir} \ge 150 \, {\rm km \ s^{-1}}$  is about  $0.13 (\, h^{-1}{\rm Mpc})^{-3}$  in the CDM model we are considering. From equation (1) we see that the virial radius for  $V_{\rm cir}=150 \, {\rm km \ s^{-1}}$  is about  $20 \, h^{-1}{\rm Kpc}$  at z=3. Thus, even if each halo with  $V_{\rm cir} \gtrsim 150 \, {\rm km \ s^{-1}}$  produces a Lyman limit system everywhere within its virial radius, the total number of systems per unit redshift in one line of sight is only about 1, which is still smaller than the observed value for the LLSs

at z=3 by a factor of about 2 to 3 (see Fig.8). It is also unlikely for the LLSs at high redshifts to be produced by photoionized clouds in smaller halos. To show this we recall that the average gas density within the virial radius of a halo is  $\overline{\rho_{\rm v}}=3f_gV_{\rm cir}^2/(4\pi\,Gr_v^2)$ . Assuming ionization equilibrium we can calculate the average number density of neutral hydrogen atoms  $n_{\rm HI}$ , and it follows that the typical HI column density produced by a halo with circular velosity  $V_{\rm cir}$  is

$$N_{\rm HI} \equiv n_{\rm HI} r_v \sim 1.0 \times 10^{16} \,\rm cm^{-2} \, \left(\frac{f_g h^2}{0.0125}\right)^2 \left(\frac{1+z}{4}\right)^{9/2} \frac{(V_{\rm cir}/100 \,\rm km \, s^{-1})}{h J_{-21} T_4^{3/4} \phi},\tag{19}$$

where  $\phi$  is the volume filling factor of photoionized gas. Thus, to produce a LLS with  $N_{\rm HI} \gtrsim 10^{17} {\rm cm}^{-2}$ , the photoionized gas needs to be compressed by a factor larger than about 10 (so that  $\phi \lesssim 0.1$ ). The compression due to the hot medium, which has density given by the cooling condition (equation 5), is typically  $(T_h/T_c)(r_v/r_c)^2$ , where  $T_c$  is the temperature of the cold phase. For halos with  $V_{\rm cir} \lesssim 150 \, {\rm km \ s^{-1}}$  at z=3,  $(r_v/r_c) \lesssim 0.3$  (see Fig. 1) and  $(T_h/T_c) \lesssim 50$ , giving a compression factor of about 5 that is still too small to produce a LLS. In addition, the observations of metal line profiles show that the velocity dispersion of the individual components is near  $100 \, {\rm km \ s^{-1}}$ , indicating also that these absorption systems do not arise in very small halos.

We find that if the amplitude  $\sigma_8$  of the CDM spectrum changes from 0.67 (our standard value in the models of Fig. 8) to 1, the number of LLSs at z=3 increases by a factor of 1.6, and if we then also decrease the intensity of the ionizing background by a factor of 3, the total change in the number of LLSs is a factor of 2.5, bringing them close to what is observed. The predicted evolution is still in the opposite direction to observed, with the number of LLSs decreasing at high redshift. However, this could be due to a decreasing intensity of the ionizing background at z > 4. The number of observed quasars does not allow  $J_{-21}$  to be less than 0.2 at z=3 (e.g., Haardt & Madau 1995), but it could be lower at higher redshift.

Another possibility is that a large fraction of the observed LLSs at high redshift are produced by photoionized gas outside the virialized regions. Recent hydrodynamic simulations show that low column density absorption systems can be produced by gas in filamentary structures that arise from the gravitational collapse of initial density fluctuations giving rise to galaxies (e.g., Cen et al. 1994, Hernquist et al. 1996, Haehnelt, Steinmetz & Rauch 1996). The abundance of LLSs predicted by the SPH simulations (including an approximate treatment for self-shielding effects) was found to be substantially lower than observed, by a factor  $\sim 10$ , in Katz et al. (1996). These small number of LLSs in the simulation are produced near very high density clumps of neutral hydrogen, so few of them arise outside what we have considered here as the virialized regions in halos. The number of

systems arising in infalling regions would be increased if small clouds confined by pressure are also present in the filamentary structures found in the simulations; however, it may be difficult to obtain high enough column densities from such clouds, for the same reason why it is difficult to produce them in low-mass virialized halos: the pressure in the infall regions is low, so the photoionized gas cannot be confined to a very small volume filling factor.

This shows that in order to reproduce the observed number of LLSs, a large fraction of the mass accreting in halos needs to be baryonic, in the form of small gas clouds having a large covering factor. The fraction of 5% used in our models is a lower limit, because the number of predicted LLSs for this fraction is only as large as observed for models having the largest abundances of massive halos and the lowest values of the intensity of the ionizing background allowed by observations of quasars. The conclusion that the minimum baryon content of the clouds is larger is similar to the result obtained from the simulations of the lower column density Ly $\alpha$  forest (see Hernquist et al. 1996; Miralda-Escudé et al. 1995).

# 4.3. MgII systems

In the last subsection we have examined the rate of incidence and impact parameters for LLSs in our model. We now extend the calculation to MgII systems, and discuss the uncertainties in  $J(\nu)$  and Z, to compare with the observations that have been done so far where the absorption systems are selected from their MgII lines.

Figure 9 shows  $N_{\rm MgII}$  as a function of impact parameter for two different shapes of  $J(\nu)$ . One has  $\alpha=0.5$  without any break; the other has the same power index but with a break of a factor of 50 at  $\nu=4$  Ryd. As we can see from Fig.3, these two cases represent the two extremes. We assume a metallicity  $Z=0.3Z_{\odot}$ , and redshift z=0.5. Comparing Fig.9 with Fig.5, we see that the shape of the MgII column density profile is similar to that of HI, and the difference can easily be understood by using Fig.3. The MgII column density is, with respect to the HI column density, suppressed in halos with  $V_{\rm cir} \gtrsim 200 \, {\rm km \ s^{-1}}$ , because  $N_{\rm MgII}/N_{\rm HI}$  increases with  $\Gamma$  for  $\Gamma \lesssim 10^{-3}$ . In halos with  $V_{\rm cir} \lesssim 150 \, {\rm km \ s^{-1}}$ , where  $\Gamma$  is large, the suppression of  $N_{\rm MgII}$  is more significant for a harder UV flux spectrum (Fig. 9a).

The observed samples of MgII absorption lines select systems where the MgII line is above a threshold of equivalent width. Because the lines are usually saturated, the relation to the column density depends on how the gas along the line of sight is distributed in clouds at different velocities: larger equivalent widths will be produced for higher covering factors of the clouds at a fixed column density. Here, we shall present results for the number of absorbers and the impact parameter distribution assuming a fixed threshold  $N_{\text{MgII}} = 2 \times 10^{13} \text{cm}^{-2}$  (reasonable for W = 0.3Å; see e.g., Fig. 8 of Petitjean & Bergeron 1990), although we should bear in mind that the average cloud covering factor

can also affect the observed equivalent widths. Figure 10 shows the results for the impact parameter in halos of different  $V_{\rm cir}$ , at redshift z=0.5. The UV flux spectrum used here has parameters  $J_{-21}=0.1$ ,  $\alpha=0.5$  and  $\Theta(\nu\geq\nu_4)=0.1$  in equation (18). Comparing Fig.10 with Fig.6, we see that D depends on  $V_{\rm cir}$  in a similar manner for both MgII and HI systems. At  $V_{\rm cir}\gtrsim150\,{\rm km~s^{-1}}$ , the dependence is weaker for MgII systems, because the ratio  $N_{\rm MgII}/N_{\rm HI}$  increases with  $\Gamma$  at  $\Gamma\lesssim10^{-3}$  (see Fig.3 and §4.1). At  $V_{\rm cir}\lesssim150\,{\rm km~s^{-1}}$ , D decreases rapidly with  $V_{\rm cir}$ , due to the faster cooling rate and the lower pressures that are implied. The details of the D- $V_{\rm cir}$  relation depend on the shape of the UV flux  $J(\nu)$ , and on whether or not the systems are optically thick. The decrease of D with  $V_{\rm cir}$  at small  $V_{\rm cir}$  is slower when the UV flux is softer or as the clouds become more optically thick (Fig.3). However, the main feature in the dependence of D on  $V_{\rm cir}$  does not change for all the choices of  $N_{\rm MgII}/N_{\rm HI}$  shown in Fig.3.

The above result of impact parameter as a function of  $V_{\rm cir}$  is similar to the observational result of Steidel et al. (see Steidel 1995). The observation shows that the maximum impact parameter D of their MgII systems to the absorbing galaxies (having typically  $L_K \gtrsim 0.1 L_K^*$ ) increases slowly with the K-band luminosity  $L_K$  as  $D \propto L_K^{0.15}$ . Assuming Tully-Fisher relation  $L_K \propto V_{\rm cir}^4$ , we have  $D \propto V_{\rm cir}^{0.6}$ , which is shown in Fig.10 by the dotted line. We see that such a weak increase of D with  $V_{\rm cir}$  can be accommodated in our model, arising from the value of the cooling radius and the derived gas pressures in different halos. The very small impact parameters in low  $V_{\rm cir}$  halos agrees with the fact that MgII absorption systems are not commonly found in galaxies fainter than about  $0.1L^*$  (Steidel 1995). Our model assumes that the clouds only exist within the cooling radius, and in practice the number of clouds should decrease with radius less sharply near the cooling radius. The increase of D with  $V_{\rm cir}$  for massive halos could, therefore, be stronger. However, the number of absorption systems at large impact parameters can also be reduced, because the covering factor of clouds that can survive evaporation in the massive halos giving rise to the absorption systems at large impact parameter can be lower than unity (§3).

To see how different halos contribute to the MgII absorption, we plot in Figure 11 the cumulative number of MgII systems per unit redshift at z=0.5, produced in halos with  $V_{\rm cir} \leq V_0$ . The figure shows that most MgII systems are produced in halos with  $V_{\rm cir} = 150\text{-}300\,\mathrm{km~s^{-1}}$ . The median  $V_{\rm cir}$  is about 200 km s<sup>-1</sup>, which is slightly smaller than that for the LLSs (§4.2), because the ratio  $N_{\rm MgII}/N_{\rm HI}$  is reduced in massive halos due to charge transfer (Fig.3). The contribution to the total cross section made by halos with  $V_{\rm cir} \lesssim 150\,\mathrm{km~s^{-1}}$  is small, which again suggests that MgII systems should not be commonly found in the halos of dwarf galaxies.

In Figure 12, we show the total number of MgII systems and the evolution with redshift, compared to the number of Lyman limit systems, for two values of the metallicity.

The relative number of MgII systems to LLSs is correctly predicted when the metallicity is between Z = 0.1-0.3, (compared with the observational results in Steidel & Sargent 1992), and the evolution is also as observed if the metallicity in these halo clouds does not decrease very fast with redshift.

# 4.4. CIV systems

CIV is another commonly found species in QSO absorption line systems which is a high ionization species, as opposed to MgII and HI, and therefore probes regions at lower densities (e.g., Bergeron & Stasińska 1986). At present, the evidence for the connection between CIV absorbers and galaxies is still limited. Here we examine the consequence of our model for CIV absorption line systems, which may be tested by future observations.

Figure 13 shows the column density ratio  $N_{\rm CIV}/N_{\rm HI}$  for photoionized clouds as a function of the ionization parameter  $\Gamma$ . Results are shown for the same cases as shown in Fig. 3. In all cases,  $N_{\rm CIV}$  increases rapidly with  $\Gamma$  and depends only weakly on the shape of  $J(\nu)$  at  $\Gamma \lesssim 10^{-2}$ . The flattening of  $N_{\rm CIV}/N_{\rm HI}$  at  $\Gamma > 10^{-2}$  for the hardest spectrum is due to the ionization of CIV to CV. Comparing Fig. 13 with Fig. 3 we see immediately that, with respect to  $N_{\rm HI}$ ,  $N_{\rm CIV}$  should be enhanced in small halos (which have lower pressures). Figure 14 shows  $N_{\text{CIV}}$  as a function of D for halos with different  $V_{\text{cir}}$  at z=0.5. The flux  $J(\nu)$  is as specified in equation (18), with  $J_{-21}=0.1$ ,  $\alpha=0.5$  and  $\Theta(\nu\geq\nu_4)=0.1$ . Unlike HI and MgII systems, the column density profile of CIV is quite flat in large halos. The reason is that the density of CIV ions decreases rapidly to the inner region of these halos, where the pressure of gas is high and  $\Gamma$  is low. Thus, for a given halo  $N_{\rm CIV}/N_{\rm MgII}$  should increase with increasing impact parameter. For the same reason, systems with high  $N_{\rm CIV}$  are associated with small halos with  $V_{\rm cir} \sim 150\,{\rm km~s^{-1}}$ . To demonstrate this, we show in Figure 15 the impact parameter D, at which  $N_{\rm CIV}=10^{14}{\rm cm}^{-2}$  [corresponding to a rest-frame equivalent width  $W(\text{CIV}\lambda 1548) \sim 0.4 \text{Å}$  for unsaturated lines], as a function of  $V_{\text{cir}}$  for one model as specified in the figure caption. For comparison, the curve for the MgII systems in the same model (see the solid curve in Fig. 10) is included. In small halos, D is much larger for CIV systems than for MgII systems. In fact, the cross-section weighted average of  $V_{\rm cir}$  is only about  $100\,{\rm km~s^{-1}}$  for the CIV systems, but as large as about  $200\,{\rm km~s^{-1}}$  for MgII systems, in this particular model with halo density given by the CDM spectrum. Our model thus predicts that, while MgII systems are mostly associated with bright galaxies, many CIV systems should be found to be associated with small galaxies where  $N_{\text{MgII}}$  is low.

The total number of CIV systems in our model is also shown in Fig. 12; the ratio to the number of MgII systems, and the evolution with redshift, is similar to what is observed (e.g. Steidel & Sargent 1992). Unfortunately, unlike those for LLSs and MgII systems, the

number of CIV systems produced in small halos at high redshifts ( $z \gtrsim 3$ ) is not negligible, because the number of such halos is large at high redshift and CIV systems can arise in them owing to the low pressure. Thus the total number of CIV systems at high redshifts predicted by our model depends on whether or not the contribution from small halos are included. In our calculation we have neglected the contribution from halos with  $V_{\rm cir} < 50 \, {\rm km \ s^{-1}}$ . The total number of CIV systems can increase by a factor of about two, if halos with  $V_{\rm cir} \ge 30 \, {\rm km \ s^{-1}}$  are included. However, the existence of a cold phase in these small halos is uncertain, because the gas there may not be able to cool owing to photoionization heating (Efstathiou 1992; Steinmetz 1995). At  $z \gtrsim 3$ , the total number of CIV systems is smaller for metallicity  $Z = 0.3Z_{\odot}$  than for  $Z = 0.1Z_{\odot}$ , because the higher metallicity (which gives lower pressure in a halo) leads to a large ionization parameter ( $\Gamma \gtrsim 0.1$ ) in small halos so that the ratio between CIV column density and the total hydrogen column density decreases with increasing  $\Gamma$  (see Fig. 13 where  $N_{\rm CIV}/N_{\rm HI}$  is shown).

Observations of QSO metal line systems at  $z \sim 1$  have shown that a large fraction ( $\sim 70\%$ ) of metal line systems are "CIV-only" ones (with rest-frame equivalent width  $W \gtrsim 0.3 \text{Å}$ ) in which MgII systems (with the same equivalent-width limit) are not detected, while there is only a small fraction of MgII systems where CIV is not observed (Steidel & Sargent 1992). According to our model, the first result is understood mainly from the fact that small halos have much larger cross sections for CIV absorption than for MgII absorption (Fig. 15). The second observational result is, however, not implied by our model based on the photoionized phase, because systems in the most massive halos should show only MgII absorption without detectable CIV, owing to the high pressures that are prevalent everywhere within the cooling radius. There are essentially two ways to produce CIV absorption in these massive halos. The first is to have some gas in the cold phase in regions of lower pressure, probably outside the cooling radius  $r_c$ . Our simplified model assumes that no gas is present in the cold phase at  $r > r_c$ , but in a realistic model the density of photoionized gas would decline more smoothly with radius, which would allow for more CIV to be produced in the outer regions.

The other possible origin of CIV systems in massive halos is from collisionally ionized gas. Although the gas in the hot phase is too hot to produce detectable CIV (see §4.5), "warm gas" (with temperature between the halo virial temperature and the photoionization-equilibrium temperature), which is in the process of cooling after being shocked or in heat conduction fronts between the hot and the cold phase (e.g., Borkowski, Balbus, & Fristrom 1990), should give rise to CIV. The fraction of carbon atoms that are in CIV in collisionally ionized gas peaks at 0.3 at temperatures (1-2.5)  $\times 10^5$  K. Since the total hydrogen column density of the hot phase at an impact parameter  $D \lesssim 30$  Kpc is typically  $10^{20}$  cm<sup>-2</sup> for halos with  $V_{\rm cir} \sim 250$  km s<sup>-1</sup> at  $z \sim 1$ , the typical CIV column density in

the warm phase is  $N_{\rm CIV} \sim (f_w Z/Z_\odot) 10^{16} {\rm cm}^{-2}$ , where  $f_w$  is the total mass of warm gas in units of that of the hot gas. The maximum amount of gas that could be present in this warm phase is obtained by assuming that a significant fraction of the cooling energy from the hot phase is emitted in conduction fronts. This would decrease the pressure of the hot phase, since the effective cooling rate is increased. Assuming pressure equilibrium, it then follows that  $f_w \sim E_w \Lambda(T_h) T_w / \Lambda(T_w) T_h$ , where  $E_w$  is the fraction of the cooling radiation emitted from the warm phase,  $\Lambda(T)$  is the cooling rate at temperature T, and  $T_h$  and  $T_w$  are the temperatures of the hot and the warm phases, respectively. To estimate  $E_w$ , we have calculated a simple plane-parallel, stationary conduction front between temperatures  $T_c = 10^4 {\rm K}$  and  $T_h = 2 \times 10^6 {\rm K}$  (see Zel'dovich & Pickelner 1969). This shows that the fraction of energy emitted at temperatures  $(1\text{-}2.5) \times 10^5 {\rm K}$  can be at most 20%. Thus,  $f_w \lesssim 10^{-3}$ , so the CIV column densities in massive halos from collisionally ionized gas should only be  $\sim 3 \times 10^{12} {\rm cm}^{-2}$  (for  $Z = 0.3 Z_\odot$ ), suggesting that CIV is mostly produced in the photoionized phase.

## 4.5. The hot phase and highly ionized systems

For even more highly ionized species like OVI, our model also predicts that they cannot be due to photoionized clouds in massive galactic halos, because the ionization parameter is too low to produce such ionization states. The long dashed curve in Fig. 15 shows the impact parameter at which  $N_{\rm OVI}=10^{14}{\rm cm}^{-2}$ . It is clear that such OVI systems should not be commonly found as photoionized clouds in halos with  $V_{\rm cir}\gtrsim 150\,{\rm km~s^{-1}}$ . The necessity for a collisionally ionized component to explain some of the OVI lines has also been discussed in Giroux, Sutherland, & Shull (1994). Some OVI might arise from an intermediate temperature phase as discussed above, but the column densities are expected to be low, for the same reason that they are low for CIV. Here we consider the possibility of producing highly ionized species from the hot phase in our model.

Given the density and temperature profiles (see equations 3 and 4) of the hot phase, we can calculate the column densities of different ions at any specific impact parameter. At the temperature of the hot phase (typically about  $10^6$ K for galactic-sized halos), most of the gas is in highly ionized species, and the strongest lines that are produced in the UV are caused by lithium-like ions (e.g. CIV, NV, OVI, NeVIII and MgX). Mulchaey et al. (1996) suggest that such highly ionized species in QSO absorption spectra can be used as a probe for a hot medium in groups of galaxies. Here we examine whether these species have high enough column densities in our model to be detected by observations. As before we use the code CLOUDY to calculate the relative column densities. The results of the column densities at a fixed impact parameter  $D = 20 h^{-1}$ Kpc as a function of halo circular velocity

are shown in Figure 16 for the species mentioned above. (We note that the column densities depend only weakly on D for  $D = 10\text{-}30\,h^{-1}\mathrm{Kpc}$  in halos with  $V_{\mathrm{cir}} > 150$ .) For comparison the HI column density given by the hot phase is also plotted. The column densities of the metal species are proportional to the metallicity of the hot gas, and we have assumed a metallicity of  $0.1Z_{\odot}$  in our calculation. Since our results do not depend strongly on redshift, only those for halos at z=2 are shown.

It is clear from Fig. 16 that strong absorption lines are not expected for any of these species. At the maximum column densities shown in Fig. 16, the predicted rest-frame equivalent width (in doublet) is about 0.1Å for OVI and 0.01-0.02Å for the other metal species. Thus, while the equivalent width for OVI is already close to the detection limit of HST, especially when the metallicity is larger than  $0.1Z_{\odot}$ , the equivalent widths for the other species are still too small to be detectable. For halos at high redshifts, the predicted equivalent width for OVI should be readily detectable by the HIRAS echelle spectrograph on the Keck Telescope. To test for the presence of the hot phase postulated in our model, high resolution observations of OVI lines would be needed to distinguish between gas in the photoionized and the hot phase, from the width of the individual component lines. A wide, smooth component in OVI absorption lines would be indicative of the hot phase, and would also give invaluable information about the dynamical state of the hot halo gas from a measurement of the hydrodynamic broadening. However, these observations are difficult because the OVI lines are superposed with the Ly $\alpha$  forest. Weymann (1995) suggests that the hot gas in galactic halos might also produce some weak broad Ly $\alpha$  lines. As we see from Fig. 16, the HI column density is extremely low in our model, because we have assumed that the hot gas in a halo has temperature similar to the virial temperature of the halo.

# 5. Discussion and Summary

A model has been constructed where QSO metal absorption line systems are produced in a halo of gas that was accreted into dark matter halos and was shocked, forming a hot phase, and contains also a photoionized phase in the form of clouds moving through the halo. The clouds could either form from cooling of the diffuse hot gas, or could form from inhomogeneities in the infalling material when the gas is shocked, or be stripped from denser gas in satellite galaxies. As they move through the hot gas falling in the gravitational potential well, the clouds should accumulate in the centers of dark halos and probably form gaseous disks and stars. The absorption line systems we have modeled are caused by the clouds as they move in towards the center, before they are aggregated on a forming galaxy. Thus, the properties of the 'halo gas' uncovered by absorption line studies are essential for our understanding of galaxy formation. Equation (10) implies an average accretion rate of

about several solar masses per year for a typical galaxy with  $V_{\rm cir} \sim 200 \, \rm km \ s^{-1}$ , which in turn implies a total gas mass of about  $10^{10}$ - $10^{11}M_{\odot}$  for these galaxies, consistent with the mass of the disk of our galaxy. The properies of galaxies formed in this way may depend crucially on the state in which cold gas was accreted into the halos. In low-mass halos where the cooling time is short, most of the accreted gas may merge directly to the center and dissipate its energy quickly, forming stars in cloud collisions, and perhaps producing irregular galaxies. In more massive halos where the cooling time is longer, accreted gas may be first incorportated into a hot halo and then cool to form cold clouds moving in a more regular way to the center, probably forming a disk. It is therefore important to see the differences in the properties of the absorption-line systems around different galaxies. The cold gas accumulated in the center of a halo may settle down to a rotationally supported gaseous disk (or, in some cases, be partially supported as well by random motion and thermal pressure), and produce the observed damped Lyman alpha systems (see e.g., Wolfe 1995). The amount of gas observed in such systems suggests that most of the gas that collapsed in halos of  $V_{\rm cir} \gtrsim 50 \, {\rm km~s^{-1}}$  at  $z \sim 3$  should stay in gaseous form (Mo & Miralda-Escudé 1994; Kauffmann & Charlot 1994). Since damped Lyman alpha systems at z>2 are observed to be metal poor  $(Z<0.1Z_{\odot})$ , see Pettini et al. 1995), the clouds in galactic halos at  $z \gtrsim 2$  should also be metal poor. The 'halo gas' must be more enriched at lower redshifts to produce the observed metal line systems with higher metallicity. It is unclear at present how the gas in galactic halos was enriched. It is possible that galactic halos at low redshifts contain much gas that belonged previously to the interstellar medium of satellite galaxies, or originated from supernova explosions during the onset of star formation in the halo center.

Much theoretical work remains to be done to see the plausibility of our model and to make it more predictive, mainly to understand the physical processes determining the rate of formation and destruction of gas clouds moving through the halo, the distribution of cloud masses and velocities, etc. Many simplifications have been necessary in this paper, but within the model uncertainties we have found that the principal characteristics of LLSs and metal line absorption systems can be reproduced by the accreted material that forms the galaxies, in the form of clouds in pressure equilibrium with hot halo gas, photoionized by the extragalactic background. The main results are as follows:

- (1) The masses of the clouds are in the range  $10^5$ - $10^6 M_{\odot}$ , when constrained to have a covering factor of about unity along a line of sight in typical halos with circular velocity  $V_{\rm cir} \sim 200\,{\rm km~s^{-1}}$  and within an impact parameter  $\sim 30\,h^{-1}{\rm Kpc}$ , as is observed for the QSO MgII systems. Their typical sizes are near 1 Kpc, and the neutral fractions are  $\sim 0.02$ . Such clouds are stable against both gravitational collapse and heat conduction.
  - (2) The clouds in galactic halos can be the origin of most absorption line systems with

HI column densities  $N_{\rm HI} \gtrsim 10^{17} {\rm cm}^{-2}$  at redshifts  $z \lesssim 2$ ; however, at  $z \simeq 3$ , the number of such systems predicted by our model is lower than observed. The number of absorption systems can be brought into agreement with observations only if the intensity of ionizing radiation is as low as allowed by the observations of the number of quasars, and the fraction of mass accreting in halos which is baryonic and in gaseous form is larger than 5%.

- (3) For a typical halo with circular velocity  $V_{\rm cir} \sim 200\,{\rm km~s^{-1}}$ , the HI and MgII column densities decline rapidly with impact parameter as a result of the pressure gradient in the halo. CIV systems are more abundant at large radius because the higher pressure in the inner parts of halos leads to lower ionization states. At redshifts  $z \sim 0.5$ , the maximum impact parameter for producing a system with  $N_{\rm HI} \sim 10^{17} {\rm cm^{-2}}$  is near  $40\,h^{-1}{\rm Kpc}$  in halos with  $V_{\rm cir} \gtrsim 200\,{\rm km~s^{-1}}$ , increasing slowly with  $V_{\rm cir}$ ; it decreases abruptly at  $V_{\rm cir} \lesssim 200\,{\rm km~s^{-1}}$ . This result also applies to MgII systems with column density  $N_{\rm MgII} = 10^{13} \cdot 10^{14} {\rm cm^{-2}}$ , depending on the metallicity of these systems. The observed cutoff of MgII systems at impact parameters  $\gtrsim 40\,h^{-1}{\rm Kpc}$  can arise as a result of the cooling radius and the pressure gradient (through the effect on the neutral fraction in the clouds) of gas in galactic halos.
- (4) Photoionized clouds should not be abundant at large radius from massive halos, where the gas is virialized but the cooling time is long. If photoionized clouds were present with a large covering factor in regions where the cooling time is long, massive clusters today would contain most of the Lyman limit systems, which would show strong negative evolution due to the recent formation of clusters.
- (5) Most LLSs and MgII systems at low redshifts are associated with massive halos in normal bright galaxies, while most CIV systems should be found in the halos of small galaxies and in the outer regions of big halos.
- (6) The hot phase in galactic-sized halos can give rise to detectable absorption lines in OVI, while the column densities predicted for other highly ionized species are low and difficult to observe.

Further observations of absorption line systems and their relation to galaxies should open a new era in our understanding of how galaxies form, as the physical conditions of the gas in the halos around galaxies, and the dependence of these conditions on galaxy luminosity and morphology are unravelled.

We thank John Bahcall, Cedric Lacey and Simon White for useful discussions. We also thank Gary Ferland for providing us with the photoionization code CLOUDY. JM is supported by the W. M. Keck Foundation and by NASA grant NAG-51618, and HM by the Ambrose Monell Foundation. We also acknowledge support from NSF grant PHY94-07194

in the Institute for Theoretical Physics in Santa Barbara.

### REFERENCES

Anninos P., Norman M., 1995, preprint

Bahcall J.N., et al. 1995, ApJS, in press

Bahcall J.N., Spitzer L., 1969, ApJ, 156, L63

Balbus S.A., 1991, ApJ, 372, 25

Balbus S.A., Soker N., 1989, ApJ, 341, 611

Bardeen J.M., Bond J.R., Kaiser N., Szalay A.S., 1986, ApJ, 304, 15

Bechtold J., Ellingson E., 1992, ApJ, 396, 20

Begelmann M. C., McKee C.F., 1990, 358, 375

Bergeron J., 1995, in QSO Absorption Lines, ed. G. Maylan, Springer: Berlin, p.127

Bergeron J., Boissé P., 1991, A&A, 243, 344

Bergeron J., Cristiani S., Shaver P., 1992, A&A, 257, 417

Bergeron J., Stasińska G., 1986, A&A, 169, 1

Borkowski K.J., Balbus S.A., Fristrom C.C., 1990, ApJ, 355, 501

Cen R.Y., Miralda-Escudé J., Ostriker J.P., Rauch M.R., 1994, ApJ, 437, L9

Cowie L.L., McKee C.F., 1977, ApJ, 211, 135

Dean J.F., Davies R.D., 1975, MNRAS, 170, 503

Efstathiou G., 1992, MNRAS, 256, 43P

Evrard A.E., 1990, ApJ, 363, 349

Fabian A., 1994, ARA&A, 32, 277

Fall M., Rees M.J., 1985, ApJ, 298, 18

Ferland G., 1993, University of Kentucky Department of Physics and Astronomy Internal Report

Ferrara A., Field G.B., 1994, ApJ, 423, 665

Giroux, M. L., Sutherland, R. S., & Shull, M. J. 1994, ApJ, 435, L97

Gunn J., 1982, in Astrophysical Cosmology, ed. H.A. Brück, G.V. Coyne & M.S. Longair, Pontifical Academy of Sciences: Vatican, p233 Haardt F., Madau P., 1995, submitted to ApJ

Haehnelt M., Steinmetz M., Rauch M., 1996, ApJ, submitted

Hernquist L., Katz N., Weinberg D.H., Miralda-Escudé J., 1996, ApJ, 457, L51

Jakobsen P., Boksenberg A., Deharveng J.M., Greenfield P., Jedrzejewski R., Paresce F., 1994, Nat, 370, 35

Kang, H., Shapiro, P. R., Fall, S. M., & Rees, M. J. 1990, 363, 488

Katz N., Weinberg D.H., Hernquist L., Miralda-Escudé J., 1996, ApJ, 457, L57

Kauffmann G., Charlot S., 1994, ApJ, 430, L97

Lacey C., Cole S., 1993, MNRAS, 262, 627

Loewenstein M., 1989, MNRAS, 238, 15

Loewenstein M., 1990, ApJ, 349, 471

Madau P., 1992, ApJ, 389, L1

Managoli A., Rosner R., Fryxell B., 1990, MNRAS, 247, 367

McCammon D., Sanders W.T., 1984, ApJ, 287, 167

McKee C.F., Cowie L.L., 1977, ApJ, 215, 213

Miralda-Escudé J., Cen R.Y., Ostriker J.P., Rauch M., 1995, submitted to ApJ

Miralda-Escudé J., Ostriker J.P., 1990, ApJ, 350, 1

Mo H.J., 1994, MNRAS, 269, L49

Mo H.J., Miralda-Escudé J., 1994, ApJ, 430, L25

Mo H.J., Miralda-Escudé J., Rees M.J., 1993, MNRAS, 264, 705

Mulchaey J., Mushotzky R.F., Burstein D., Davis D.S., 1996, ApJ, 456, L1

Murray S.D., White S.D.M., Blondin J.M., Lin D.N.C., 1993, ApJ, 407, 588

Navaro J., Frenk C., White S.D.M., 1995, MNRAS, in press

Nulsen P.E.J., 1986, MNRAS, 221, 377

Peebles P.J.E., 1980, The Large-Scale Structure of the Universe, Princeton University Press: Princeton

Pettini M., King D.L., Smith L.J., Hunstead R.W., 1995, in QSO Absorption Lines, ed. G. Meylan, Springer: Berlin, p.71

Petitjean P., Bergeron J., 1990, A&A, 231, 309

Petitjean P., Bergeron J., Puget J.L., 1992, A&A, 265, 375

Press W.H., Schechter P., 1974, ApJ, 187, 425

Sargent W.L.W., Steidel C.C., Boksenberg A., 1989, ApJ, 334, 22

Spitzer L., 1978, Physical Processes in the Interstellar Medium, Wiley: New York

Steidel C.C., 1990, ApJS, 74, 37

Steidel C.C., 1993, in The Environment and Evolution of Galaxies, eds. J.M. Shull and H.A. Thronson, Kluwer: Dordrecht, p.263

Steidel C.C., 1995, in QSO Absorption Lines, ed. G. Meylan, Springer: Berlin, p.137

Steidel C.C., Sargent W.L.W., 1992, ApJS, 80, 1

Steinmetz M., 1995, preprint

Stengler-Larrea E.A., et al. 1995, ApJ, 444, 64

Storrie-Lombardi L.J., McMahon R.G., Irwin M.J., Hazard C., 1994, ApJ, 427, L13

Sutherland R.S., Dopita M.A., 1993, ApJS, 88, 253

Tabor G., Binney J., 1993, MNRAS, 263, 323

Tenorio-Tagle G., Rozyczka M., Bodenheimer P., 1990, A&A, 237, 207

Vogel S., Reimers D., 1995, A&A, 294, 377

Walker T.P., Steigman G., Schramm D.N., Olive K.A., Kang H-S., 1991, ApJ, 376, 51

Wang Q., McCray R., 1993, ApJ, 409, L37

Waxman E., Miralda-Escudé J., 1995, ApJ, 451, 451

Weymann R.J., 1995, in QSO Absorption Lines, ed. G. Meylan, Springer: Berlin, p.3

White S.D.M., 1995, in 1993 Les Houches Lectures, ed. R. Schaeffer, in press

White S.D.M., Rees M.J., 1978, MNRAS, 183, 341

Wolfe A., 1995, in QSO Absorption Lines, ed. G. Meylan, Springer: Berlin, p.13

Yanny B., York D.G., Williams T.B., 1990, ApJ, 351, 377

Zel'dovich Ya. B., Pikel'ner S.B., 1969, Soviet Phys. JETP, 29, 170

This preprint was prepared with the AAS IATEX macros v4.0.

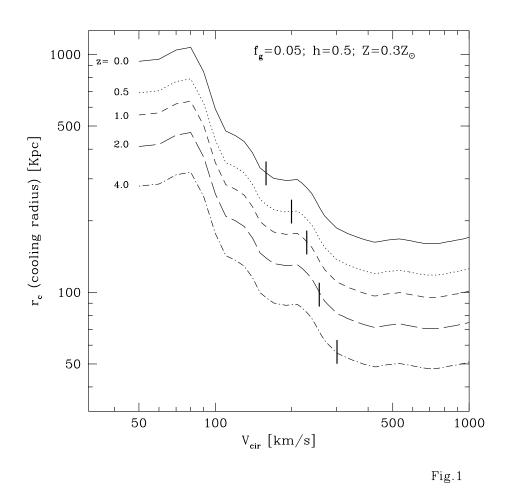


Fig. 1.— Cooling radius as a function of halo circular velocity, shown at different redshifts z. The vertical marks show the value of  $V_{\rm cir}$  where the cooling radius is equal to the virial radius. For lower  $V_{\rm cir}$ , all the gas in the virialized halo cools on a time shorter than the age of the halo, while at higher  $V_{\rm cir}$  the cooling time is longer. Result is show for a model with  $f_g = 0.05$ , h = 0.5 and with metallicity  $Z = 0.3Z_{\odot}$ . The cooling function is adopted from Sutherland & Dopita (1993).

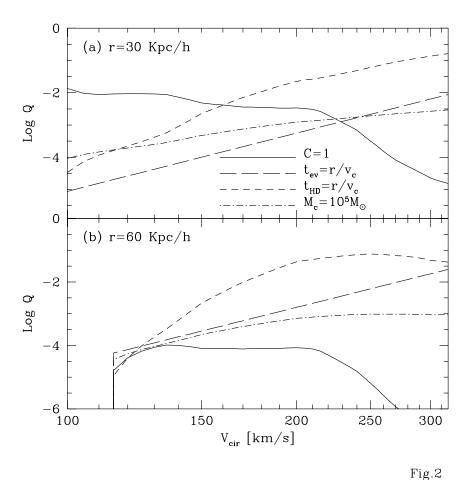


Fig. 2.— The allowed value of Q, defined as the ratio between the mass of cloud and the critical mass for gravitational collapse, for clouds located at (a)  $r = 30 \, h^{-1} \rm Kpc$  and (b)  $r = 60 \, h^{-1} \rm Kpc$  from the centers of halos with different  $V_{\rm cir}$ . The solid curve shows the value of Q, below which the covering factor of clouds C > 1. The long dashed (short dashed) curve shows the limit of Q, above which the cloud will not be disrupted by heat conduction (hydrodynamic instability) as it moves through the halo over a radius r. The dot-dashed curve shows a constant cloud mass:  $M_c = 10^5 M_{\odot}$ . Result is shown for halos at redshift z = 0.5. We also assume  $f_g = 0.05$ ,  $Z = 0.3 Z_{\odot}$  and  $v_c = V_{\rm cir}$ .

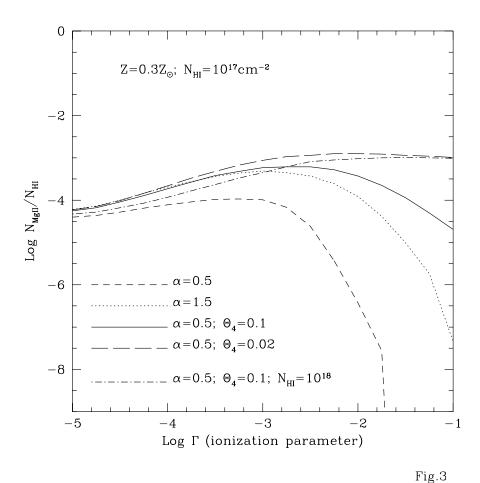


Fig. 3.— The ratio between MgII and HI column densities as a function of the ionization parameter  $\Gamma$  (defined as the ratio between the number density of photon above the hydrogen Lyman limit frequency and the number density of total hydrogen), for various shapes of the UV flux, as specified by the power index  $\alpha$  and  $\Theta_4 \equiv \Theta(\nu \geq \nu_4)$ . The dot-dashed curve shows the result for clouds with  $N_{\rm HI} = 10^{18} {\rm cm}^{-2}$ , while other curves show results for clouds with  $N_{\rm HI} = 10^{17} {\rm cm}^{-2}$ . For all cases a metallicity  $Z = 0.3 Z_{\odot}$  is used.

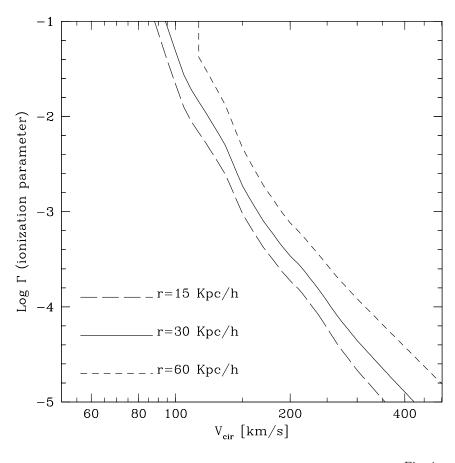


Fig.4

Fig. 4.— The ionization parameter  $\Gamma$  of pressure confined clouds located at a radius r from halo center, as a function of halo circular velocity. Results are shown for three typical radius in halos at z=0.5, with  $f_g=0.05$  and  $Z=0.3Z_{\odot}$ .

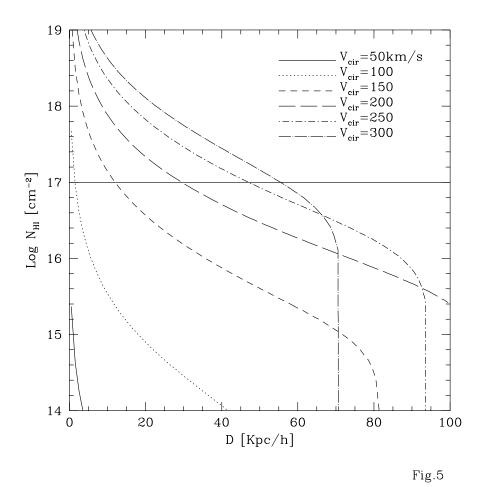


Fig. 5.— HI column density as a function of impact parameter D, for halos at z=0.5 and with various  $V_{\rm cir}$ . The model parameters are  $f_g=0.05, Z=0.3Z_{\odot}$  and  $v_c=V_{\rm cir}$ . The horizontal line indicates  $N_{\rm HI}=10^{17}{\rm cm}^{-2}$ , above which a Lyman limit system is produced.

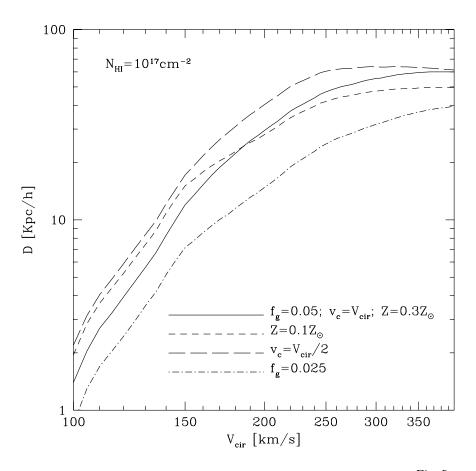


Fig.6

Fig. 6.— The impact paramter D, at which  $N_{\rm HI}=10^{17}{\rm cm}^{-2}$ , as a function of halo circular velocity. The solid curve shows the result for the 'fiducial' model with  $f_g=0.05,\,Z=0.3Z_\odot$  and  $v_c=V_{\rm cir}$ ; each other curve shows the result for a model in which one model parameter differs from that for the fiducial model, as indicated in the panel. Results are shown for halos at z=0.5. The UV flux has  $J_{-21}=0.1,\,\alpha=0.5$  and  $\Theta_4=0.1$ .

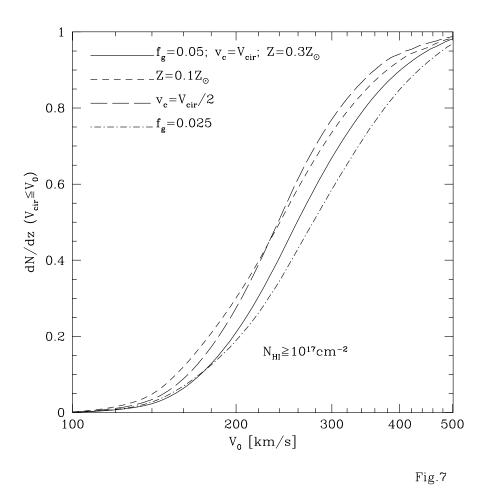


Fig. 7.— Cumulative cross section for absorption systems with  $N_{\rm HI} \geq 10^{17} {\rm cm}^{-2}$  at z=0.5, given by halos with circular velocity  $V_{\rm cir} \leq V_0$ , as a function of  $V_0$ . The total cross section has been normalized to be 1. The results are shown for the same models as those in Figure 6.

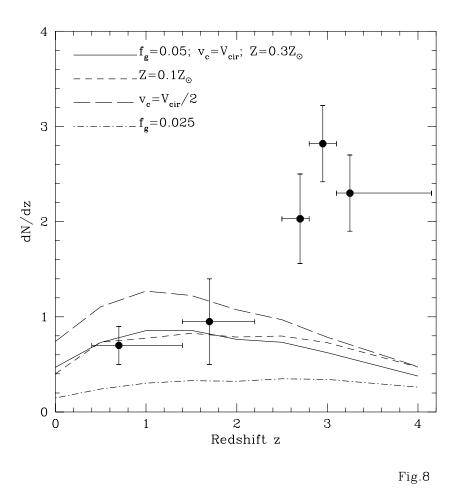


Fig. 8.— The number of  $N_{\rm HI} \geq 10^{17} {\rm cm}^{-2}$  absorption systems per unit redshift, as a function of redshift z. Curves show theoretical models; data points show the observational result for Lyman limit systems, adopted from Stengler-Larrea et al. (1995). Results are shown for the same models as those in Figure 6. The dependence of UV flux on z is that specified in the text.

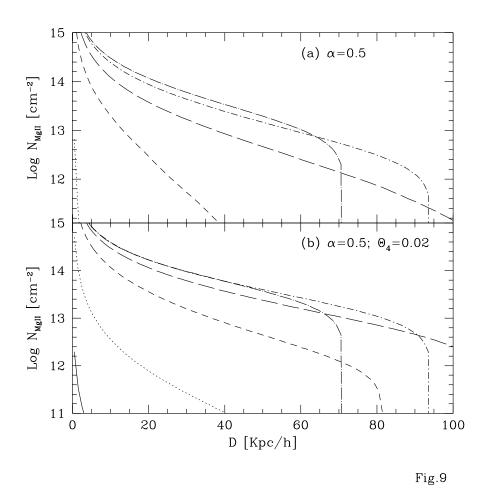


Fig. 9.— The MgII column density as a function of impact parameter, for halos at z=0.5 and with circular velocity  $V_{\rm cir}=50$  (solid curve), 100 (dotted curve), 150 (short dashed curve), 200 (long dashed curve), 250 (dotted-short-dashed curve), 300 km s<sup>-1</sup> (dotted-long-dashed curve), in a model with  $f_g=0.05$ ,  $Z=0.3Z_{\odot}$  and  $v_c=V_{\rm cir}$ . Results are shown for two models of UV flux, one is a power law with  $\alpha=0.5$ , the other has the same power index but with a break at 4 Ryd so that  $\Theta_4\equiv\Theta(\nu\geq\nu_4)=0.02$ . In both cases  $J_{-21}=0.1$ .

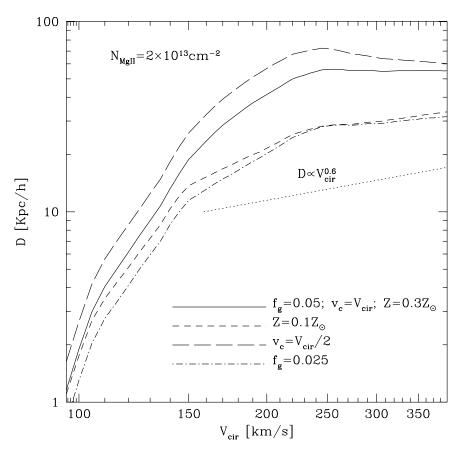


Fig.10

Fig. 10.— The impact parameter D, at which  $N_{\rm MgII} = 2 \times 10^{13} {\rm cm}^{-2}$ , as a function of halo circular velocity. Results are show for halos at z=0.5, and for the same models as shown in Figure 6. The dotted line shows the relation  $D \propto V_{\rm cir}^{0.6}$ , for the reason discussed in the text.

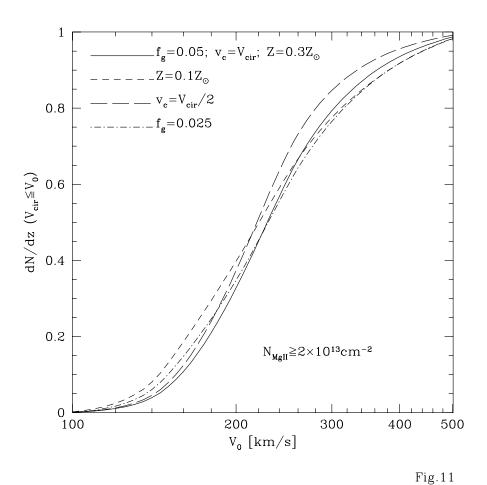


Fig. 11.— Cumulative cross section of MgII systems at z=0.5, with  $N_{\rm MgII} \geq 2 \times 10^{13} {\rm cm}^{-2}$ , given by halos with circular velocity  $V_{\rm cir} \geq V_0$ , as a function of  $V_0$ . Results are shown for the same models as those in Figure 6.

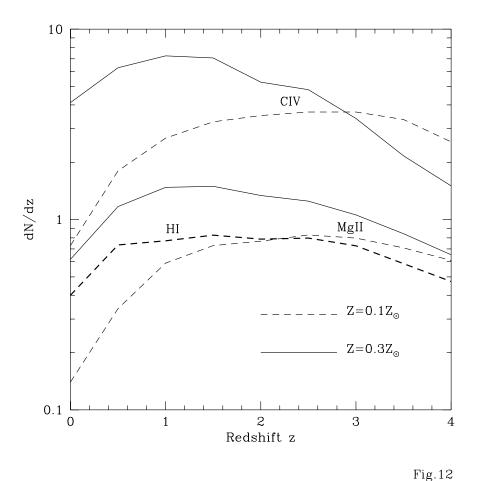


Fig. 12.— The number of CIV systems with  $N_{\rm CIV} \geq 10^{14} {\rm cm}^{-2}$  and that of MgII systems with  $N_{\rm MgII} \geq 2 \times 10^{13} {\rm cm}^{-2}$  per unit redshift, as a function of redshift z. Results are shown for two models. One (shown by the solid curves) has  $f_g = 0.05$  and  $v_c = V_{\rm cir}$  with  $Z = 0.3 Z_{\odot}$ , wheras the other (shown by the dashed curves) has the same  $f_g$  and  $v_c$  but with  $Z = 0.1 Z_{\odot}$ . The dependence of the UV flux on redshift is as specified in the text. For comparison the result for the HI systems with  $N_{\rm HI} \geq 10^{17} {\rm cm}^{-2}$  in the latter model is shown by the thick dashed curve.

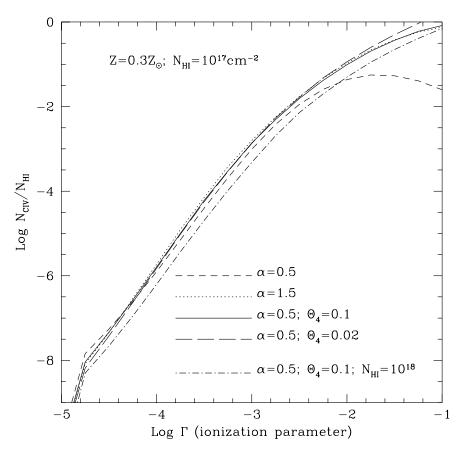


Fig.13

Fig. 13.— The ratio between CIV and HI comlun densities as a function of the ionization parameter, for various shapes of UV flux. Results are shown for the same cases as those shown in Figure 3.

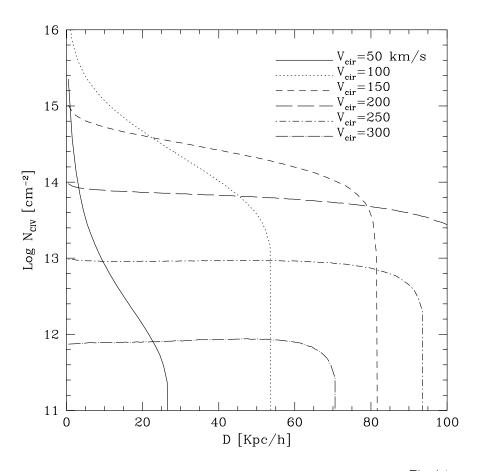


Fig.14

Fig. 14.— The CIV column density as a function of impact parameter, for halos at z=0.5 and with different circular velocities, in a model with  $f_g=0.05,~Z=0.3Z_{\odot}$  and  $v_c=V_{\rm cir}$ . The UV flux has  $J_{-21}=0.1,~\alpha=0.5$  and  $\Theta_4=0.1$ .

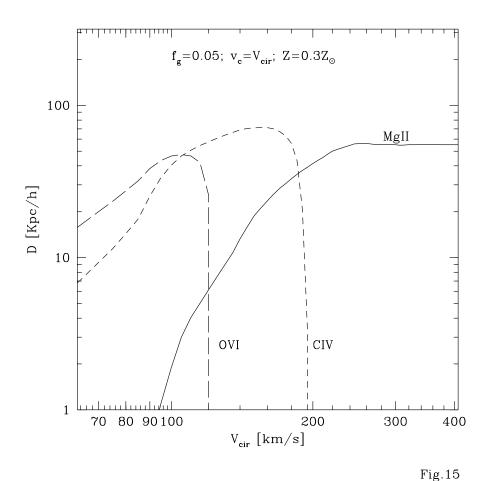


Fig. 15.— The impact parameters at which the CIV column density  $N_{\rm CIV}=10^{14}{\rm cm}^{-2}$  (short dashed curve) and the OVI column density  $N_{\rm OVI}=10^{14}{\rm cm}^{-2}$  (long dashed curve), as a function of halo circular velocity  $V_{\rm cir}$ . Results are shown for halos at z=0.5, in a model

with  $f_g = 0.05$ ,  $Z = 0.3Z_{\odot}$  and  $v_c = V_{\rm cir}$ . The UV flux has  $J_{-21} = 0.1$ ,  $\alpha = 0.5$  and  $\Theta_4 = 0.1$ . For comparison, the parameter at which  $N_{\rm MgII} = 2 \times 10^{13} {\rm cm}^{-2}$  (shown in Figure 10) is also plotted here as the solid curve.

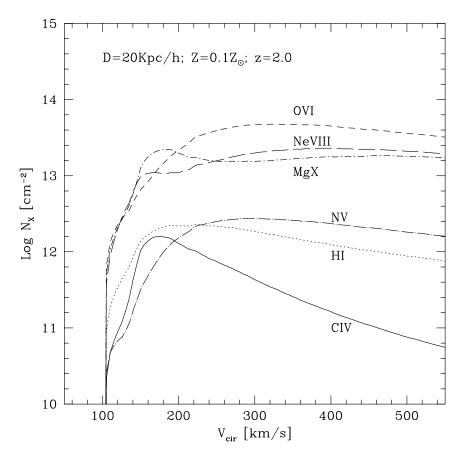


Fig. 16

Fig. 16.— The column densities (at an fixed impact parameter  $D=20\,h^{-1}{\rm Kpc}$ ) of different ions arising from the hot phase in halos as a function of halo circular velocity  $V_{\rm cir}$ . Results are shown for halos at z=2. We have assumed  $f_g=0.05$  and a metallicity of  $0.1Z_{\odot}$  for the hot gas.